Journal of *Marine Science and Engineering*

MDPI

Article

Uncertainty in the Assessment of Wave Overtopping in Mediterranean Moroccan Ports Associated with Climate Change

Raghda Jebbad [1,*], Joan Pau Sierra [1,2], Xavier Gironella [1,2], Cesar Mösso [1,2], Daniel González-Marco [1,2] and Piero Lionello [3]

[1] Laboratori d'Enginyeria Marítima, Universitat Politècnica de Catalunya BarcelonaTech, Jordi Girona 1-3, 08034 Barcelona, Spain; joan.pau.sierra@upc.edu (J.P.S.); xavi.gironella@upc.edu (X.G.); cesar.mosso@upc.edu (C.M.); daniel.gonzalez-marco@upc.edu (D.G.-M.)
[2] Centre Internacional d'Investigació dels Recursos Costaners (CIIRC), Jordi Girona 1-3, 08034 Barcelona, Spain
[3] Dipartimento di Scienze e Tecnologie Biologiche e Ambientali (DiSTeBA), University of Salento, 73100 Lecce, Italy; piero.lionello@unisalento.it
* Correspondence: raghda.jebbad@upc.edu

Abstract

This study examines the impact of climate change on wave overtopping discharge (q) at eight Moroccan Mediterranean ports, under climate scenarios SSP2-4.5 and SSP5-8.5, projected to the year 2100. To address inter-model variability and better represent future conditions, wave data from four different models were used. The analysis considers three return periods—1, 5, and 25 years—and includes both central estimates and values from the 90% confidence intervals to assess uncertainty from sea level rise (SLR) and wave projections. Results show that overtopping discharges increase with return period, along with the number of ports affected. At 1 year, two ports exceed tolerable thresholds; at 5 years, three ports are impacted; and at 25 years, nearly all ports face overtopping risks. When varying SLR while holding wave height (Hs) constant, discharge variations remain within one order of magnitude. However, when varying Hs with constant SLR, variations span two to three orders of magnitude. These results suggest that accurate Hs projections are more critical than SLR in estimating overtopping risk, emphasizing the need to reduce wave forecast uncertainty to support climate adaptation strategies.

Keywords: wave overtopping; sea level rise; port breakwater; Morocco; wave projections

check for updates

Academic Editor: Callum R. Firth

Received: 16 September 2025
Revised: 10 October 2025
Accepted: 18 October 2025
Published: 21 October 2025

Citation: Jebbad, R.; Sierra, J.P.; Gironella, X.; Mösso, C.; González-Marco, D.; Lionello, P. Uncertainty in the Assessment of Wave Overtopping in Mediterranean Moroccan Ports Associated with Climate Change. *J. Mar. Sci. Eng.* **2025**, *13*, 2021. https://doi.org/10.3390/jmse13102021

Copyright: © 2025 by the authors. Licensee MDPI, Basel, Switzerland. This article is an open access article distributed under the terms and conditions of the Creative Commons Attribution (CC BY) license (https://creativecommons.org/licenses/by/4.0/).

1. Introduction

Ports are often located in coastal areas, making them highly vulnerable to natural disasters [1]. As a result, both port infrastructure and operations face increasing risks from climate-related hazards, which are expected to intensify with ongoing climate change [2]. This vulnerability can lead to operational disruptions, infrastructure damage, and economic losses [3]. Without significant emission reductions, climate change could cost the shipping industry up to USD 25 billion annually by century's end [4]. Since ports are key nodes in global supply chains, disruptions can have widespread ripple effects across the broader economy [5]. However, climate change impacts may not be entirely negative. For instance, increased draughts due to sea level rise (SLR) can alter wave propagation and potentially reduce siltation effects [6].

Climate change will not affect all regions equally [7]. Developing countries, especially in the Mediterranean, are expected to face disproportionate impacts. This region is warming faster than the global average [8]. Based on a global assessment of 2013 ports under high-end warming scenarios, Izaguirre et al. [9] found that African Mediterranean ports, including those in Morocco, are likely to face extremely high climate risks by 2100.

In recent years, Moroccan authorities have shown growing concern about climate change impacts on port infrastructure and operations. However, most existing research has focused on SLR and its combined effects with extreme wave conditions, particularly in relation to coastal erosion and flooding [10–12]. To our knowledge, no studies have yet addressed the specific impacts of climate change on wave overtopping at Moroccan Mediterranean ports.

Ports are exposed to future threats from SLR and potential changes in wave and storm surge patterns [13]. Rising sea levels can reduce the freeboard on docks and piers, compromising berthing and loading efficiency [14–16]. This poses safety concerns for port personnel and increases flood risk. Additionally, deeper water levels may alter wave propagation near ports [17]. Wave conditions are also influenced by shifts in wind and atmospheric pressure patterns [18], potentially disrupting operations through increased siltation, agitation, or structural stress [19].

Among the various consequences of climate change, breakwater overtopping is particularly significant for seaports [20–22]. Wave overtopping refers to the flow of water over a coastal structure, such as a breakwater. It is primarily determined by the significant wave height at the structure's toe and the available freeboard, which is the vertical distance between the still water level and the crest elevation of the structure. When incoming waves, combined with sea level conditions, exceed the available freeboard, part of the wave energy is discharged over the structure in the form of overtopping. Excessive wave overtopping can compromise port operations, damage infrastructure, and endanger people and assets located behind breakwaters [23]. In severe cases, overtopping may lead to structural failure [24].

Wave overtopping is typically assessed using empirical prediction formulas [25–27] and the artificial neural network model in EurOtop [28]. However, the results can vary significantly between models, and all prediction methods have inherent limitations due to their reliance on physical model data and associated scatter [28]. The uncertainty surrounding wave overtopping prediction methods has been extensively studied (e.g., [29–31]) and is not addressed here. Furthermore, the effects of overtopping induced by long waves are not considered here [32–34].

This study examines Moroccan Mediterranean ports, a subject that remains largely underexplored despite their acknowledged vulnerability to climate-related hazards. Research on port overtopping at a regional scale is particularly scarce in the Mediterranean, with only two studies identified in Catalonia (Spain) [20,35]. The findings from these studies, when compared with results obtained for Morocco under similar scenarios, reveal strong consistency, as both fall within the same order of magnitude. Specifically, it aims to evaluate the impacts of wave overtopping under future climate scenarios. Since overtopping discharge is largely determined by sea level and nearshore wave height [36], overtopping at several port breakwaters is analyzed by examining a range of sea level scenarios and future wave projections for various return periods. Special attention is given to assessing the uncertainty associated with each of these factors. Results show that overtopping discharges are expected to increase with return period and that wave height uncertainty exerts a greater influence on overtopping projections than sea level rise. Additionally, the ports of Kabila, Chmaala, and Cala Iris are identified as particularly vulnerable to excessive overtopping under future climate scenarios. These findings provide a scientific

basis enabling port authorities to develop targeted adaptation plans to mitigate operational and structural risks.

2. Materials and Methods

2.1. Study Area

The Alboran Sea holds a strategic position between Europe and Africa, lying between the Iberian Peninsula and North Africa and encompassing the coastal zones of Morocco and Algeria (Figure 1).

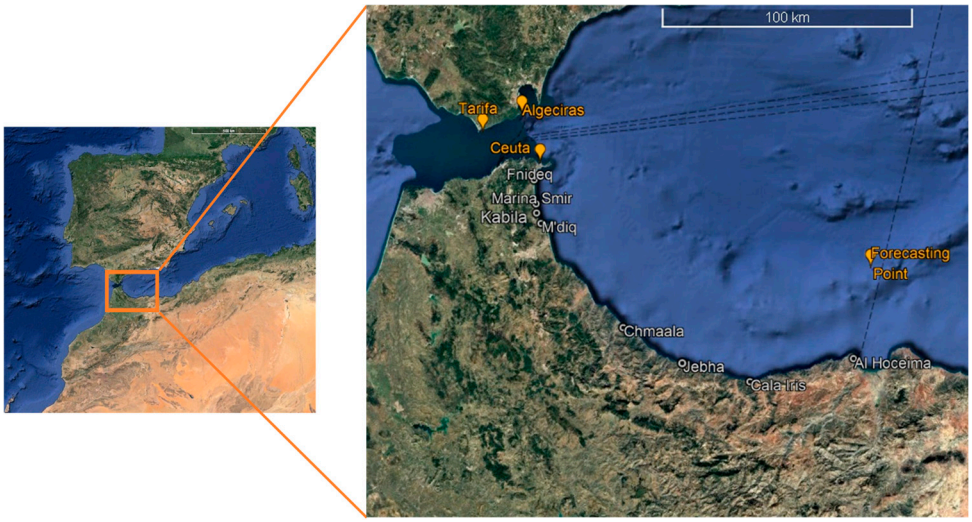

Figure 1. Location of the studied area, the analyzed ports (in white), and other points of interest (in orange).

As the westernmost basin of the Mediterranean Sea, its southern coastline stretches from the Algerian border to the Strait of Gibraltar. Tidal patterns in this region are semidiurnal [37], with relatively small tidal ranges that gradually decrease from west to east, typically between 0.8 and 1 m [38].

The Moroccan Mediterranean coast is known for its cyclogenetic nature [39]. Some storms originate in the Western Mediterranean, particularly near the Gulf of Lions, with dominant wave directions from the east (E) and east-northeast (ENE) [40]. As waves approach the coast, their energy dissipates offshore, reducing amplitude. Consequently, 90% of significant wave heights (H_s) are under 1.5 m, and only 5% exceed 3 m [39]. Typical wave periods range between 5 and 6 s, extending up to 7–11 s during storms [39], with predominant directions from the E and northeast (NE) [40].

Any change in wave climate—such as shifts in wave direction, height, or frequency—could significantly affect wave overtopping in regional ports. However, predicting future atmospheric patterns remains challenging due to complex interacting processes. Some studies anticipate wind intensification over northern Europe and weakening over Southern Europe [41,42], suggesting a decrease in Mediterranean cyclones [43] and, consequently, lower wave heights, especially in winter [42,44].

Given its location, the Alboran Sea acts as a maritime gateway between the Mediterranean and Atlantic, supporting steady maritime traffic. To accommodate this and promote economic growth, Morocco has developed 10 ports in the region. Eight of these ports were selected for this study (Figure 1) based on data availability, particularly regarding breakwater sections. Of these, one (Al Hoceima) serves passenger and cargo transport, six support fishing activities (Fnideq, M'diq, Chmaala, Jebha, Cala Iris, and Al Hoceima), and five are marinas for leisure craft (Marina Smir, Kabila, M'diq, Jebha, and Al Hoceima).

2.2. Wave and SLR Data

The acceleration of global sea level rise (SLR) since 1900 has become a growing concern, as highlighted in successive IPCC Assessment Reports. The most recent, AR6 [45], emphasizes the alarming increase in SLR, particularly between 2006 and 2018, when the rate reached 3.7 mm/year—nearly three times the 1.3 mm/year observed between 1901 and 1971. There is high confidence that the global mean sea level will continue to rise throughout the 21st century due to ongoing global warming. By 2100, projections indicate a possible rise of 0.28 to 0.55 m under the most optimistic scenario, and 0.63 to 1.60 m under the most extreme scenario, reflecting differing greenhouse gas emissions and socioeconomic pathways.

This study analyzes wave overtopping under climate change by considering two IPCC AR6 scenarios for projecting SLR to 2100, based on 10-year periods of data. The first, SSP2-4.5, represents a "middle-of-the-road" path, with emissions peaking mid-century but not reaching net-zero by 2100. The second, SSP5-8.5, outlines a high-emissions future, where CO_2 output doubles by 2050.

SLR projections were taken from the NASA AR6 Sea Level Projection Tool (https://sealevel.nasa.gov/ipcc-ar6-sea-level-projection-tool, accessed on 15 January 2025), using data for Ceuta, the nearest reference point. To incorporate tide and storm surge, the reference level for present and future scenarios was based on the 99.9th percentile from tidal gauges in Tarifa (for ports near the Strait of Gibraltar) and Melilla (for ports further east).

Three sea level scenarios were defined:

- Scenario 1: Present sea level.
- Scenario 2: SSP2-4.5—present + 0.48 m $\pm$ 90% confidence interval (0.32 m, 0.72 m).
- Scenario 3: SSP5-8.5—present + 0.69 m $\pm$ 90% confidence interval (0.51 m, 0.97 m).

To project future wave conditions, dynamic downscaling was used, combining global (GCMs) and regional circulation models (RCMs) to produce wind fields for climate scenarios. These were used to force the WAM numerical model (The WAMBDI Group, 1988), which generates wave parameters. Wave data were derived from four climate models: CMCC (Italy), CNRM (France), GUF (Germany), and LMD (France), developed under the Med-CORDEX initiative [46]. The selected scenarios—RCP 4.5 and RCP 8.5—correspond to AR5 [47] instead of AR6. This is because the authors could not obtain wave data from AR6 and had to use AR5 data. However, it should be noted that the AR5 wave scenarios used match the radiative forcing of the AR6 sea level scenarios.

The wave datasets comprise 20-year time series of significant wave height (H_s), peak wave period (T_p), and wave direction (θ), sampled every three hours at a forecasting point on the eastern boundary of the study area (see Figure 1). These datasets cover two time periods: 1985–2005 (present) and 2081–2100 (future) under RCP 4.5 and RCP 8.5.

Offshore wave data from the four models were used to define the wave extreme climate by fitting a General Extreme Value (GEV) distribution. From this, offshore wave conditions were determined for three return periods (TR): 1, 5, and 25 years, representing common and severe operational conditions and exceptional storms, respectively. This method, adapted from [20], considers all relevant directions for each port and includes 90% confidence bands.

For each return period, present and future wave conditions at the boundary point were propagated numerically to the selected ports. Propagation included H_s values from the four models (central estimate plus lower and upper bounds) for each return period and direction (between 5 and 7 directions per port). In addition, an ensemble value of *Hs* was considered for each scenario and direction, obtained by averaging the central estimates from the four models. The wave period (T_p) was calculated using a formula recommended by Puertos del Estado for

the Melilla buoy (https://bancodatos.puertos.es/BD/informes/extremales/EXT_1_1_1560.pdf, accessed on 4 February 2025), located near the forecasting point:

$$T_p = 5.32 \times (H_s)^{0.35}$$

where T_p is the peak period in seconds, and H_s is the wave height in meters.

2.3. Numerical Modeling

To propagate the offshore wave data to the breakwater location, the SWAN numerical model [48] was employed, providing *Hs*, *Tp*, and wave direction at the toe of the breakwater. Due to the size of the study area, a nesting approach was implemented. First, wave conditions (current and projected) for each return period, model, and direction were propagated from deep water using a coarse grid (0.01° resolution) to the vicinity of each port. Then, simulations were refined with a finer grid (0.0005° resolution) using boundary conditions from the coarse grid to ensure continuity. This process continued until reaching the toe of each breakwater.

The SWAN model was calibrated using buoy data from Tarifa, Algeciras, and Ceuta (Puertos del Estado). Model parameters were adjusted using real-time measurements to enhance the agreement between simulated and observed wave behavior. Calibration involved tuning the model based on various nonlinear quadruplet interactions and alternative parameterizations for whitecapping and energy dissipation due to bottom friction. Figure 2a shows an example of this calibration, and Figure 2b illustrates wave propagation on the coarse grid.

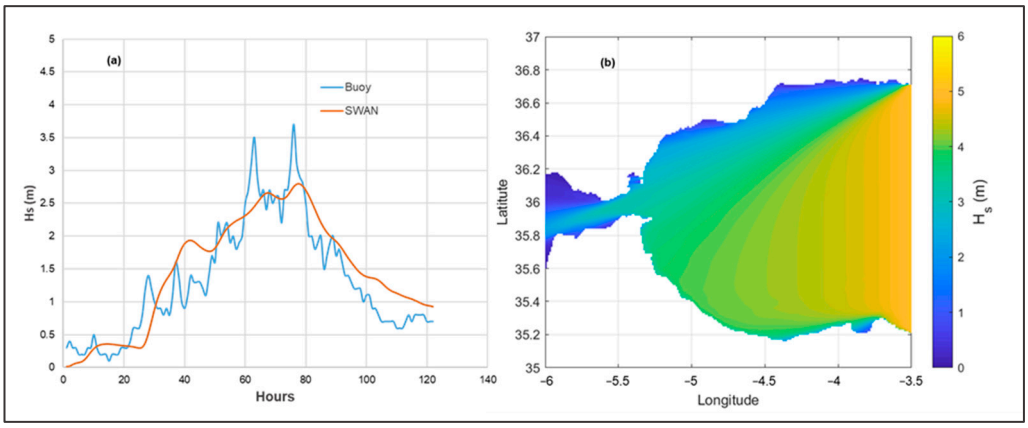

Figure 2. (**a**) Calibration of the SWAN model using Ceuta buoy data; (**b**) example of wave propagation with the SWAN model in the larger domain for waves with H_s = 5.15 m, T_p = 9.4 s, and ENE direction.

Bathymetric data for the coarse grid were sourced from GEBCO (General Bathymetric Chart of the Oceans), widely used in oceanographic studies [49]. For the finer grids and port layouts, nautical charts were used. These datasets were applied to present conditions. For future scenarios, projected sea level rise (SLR) values were added to current bathymetry to simulate future depths, and, in addition, structure freeboards were reduced by the same amount.

2.4. Overtopping Discharges

Overtopping discharges were assessed using the propagated wave parameters (H_s, T_p, and θ) and water depth at the breakwater toe. In future scenarios, breakwater freeboards were reduced by the SLR amount to reflect 2100 conditions.

The overtopping discharge was calculated using the EurOtop formula [28]:

$$\frac{q}{\sqrt{g \cdot H_s^3}} = 0.09 \cdot exp\left[-\left(1.5 \frac{R_c}{H_s \cdot \gamma_f \cdot \gamma_\beta \cdot \gamma_v}\right)^{1.3}\right]$$

where q is the overtopping discharge per unit width ($m^3/s/m$), g is gravitational acceleration, H_s is the significant wave height at the toe of the breakwater, R_c is crest freeboard of the structure, γ_f is a factor that considers the roughness and permeability of the structure, γ_β accounts for wave obliquity, and γ_v accounts for a vertical wall in the breakwater slope.

In the case of rubble mound breakwaters, this equation is applicable to steep slopes ranging from 1:2 to 4:3. The eight ports analyzed feature rubble mound breakwaters with slopes of 2:3 and 3:4, which fall within the applicable range of the formula. All ports feature a breakwater with an armour layer composed of concrete tetrapods with a density of 2400 kg/m^3. The tetrapod volumes range from 1.6 m^3 to 12.5 m^3, and none of the breakwaters include a vertical wall on either the slope or the crest.

Although it is difficult to give precise limits of tolerable overtopping [23,50], to determine if discharges are acceptable, the thresholds suggested in EurOtop [28] were applied:

- 0.3 L/s/m: for pedestrians to remain on the breakwater crest.
- 1 L/s/m: to prevent damage to breakwaters, equipment, or small boats.
- 5 L/s/m: to prevent small boats from sinking or damage to large yachts.

These thresholds are relatively strict and correspond to severe wave conditions; however, as indicated in EurOtop [28], the tolerable limits adopted for design are lower than those associated with structural failure.

A value of 0.3 L/s/m defines the threshold at which pedestrians can safely remain on the breakwater. This warning/exclusion level was established on a precautionary basis to prevent direct risks of injury or fatality, since wave overtopping may occur suddenly and with considerable violence.

The threshold of 1 L/s/m ensures that rubble mound breakwaters do not sustain damage and remain fully operational. This limit also guarantees the safety of small vessels moored behind the structure, as well as equipment located on or near the breakwater, thereby avoiding any disruption of port operations.

Finally, the limit of 5 L/s/m is intended to prevent property damage, particularly to vessels moored in close proximity to the rear side of the breakwater, which may be impacted by overtopping waves. Exceeding this threshold could lead to the sinking of small boats or significant damage to larger yachts, potentially resulting in severe economic losses.

2.5. Data Availability

Sea level rise projections were obtained from the publicly accessible NASA IPCC AR6 Sea Level Projection Tool (https://sealevel.nasa.gov/ipcc-ar6-sea-level-projection-tool, accessed on 15 January 2025). Tide gauge data for Tarifa and Melilla were accessed via Puertos del Estado (https://www.puertos.es, accessed on 4 February 2025). Wave data (significant wave height, peak period, and wave direction) were derived from four regional climate models (CMCC, CNRM, GUF, and LMD) developed under the Med-CORDEX initiative [46]. Access to these wave datasets may require institutional collaboration or direct request to the data providers. Offshore wave period (Tp) estimations used the empirical formula provided del Estado's empirical formula, using data from the Melilla buoy (https://bancodatos.puertos.es/BD/informes/extremales/EXT_1_1_1560.pdf, accessed on 4 February 2025). Bathymetric data for numerical modeling were sourced from GEBCO (https://www.gebco.net/, accessed on 18 December 2024).

All publicly available datasets used in this study can be accessed through the respective repositories as indicated. Detailed breakwater geometry data were obtained under confidentiality agreements from Moroccan governmental authorities and are not publicly available. No other proprietary datasets were used in this study.

3. Results

Figure 3 presents the overtopping discharges (q) calculated for present conditions and return periods (TR) of 1, 5, and 25 years. For each TR, q is evaluated for three significant wave height (Hs) values derived from the GEV function: the minimum from the lower confidence band across four models, the ensemble mean, and the maximum from the upper confidence band.

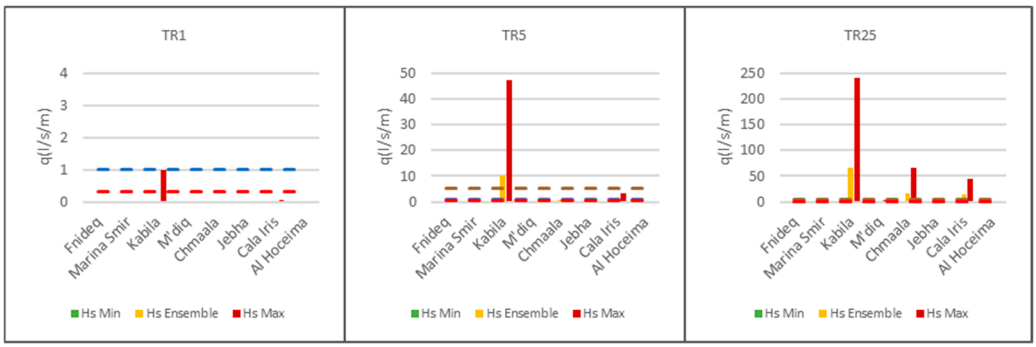

Figure 3. Overtopping discharges q for the present scenario under different return periods (TR1, TR5, and TR25), considering different wave heights. Green represents minimum wave height of the four models (lower confidence band), yellow represents ensemble wave height (average of the four models for the mean estimate), and red represents maximum wave height of the four models (upper confidence band). The dashed lines represent the operability thresholds.

For a 1-year TR, tolerable values are exceeded only in Kabila, where the discharge reaches 0.97 L/s/m for the maximum Hs. Two other ports show minimal overtopping: Chmaala (0–0.005 L/s/m) and Cala Iris (0.001–0.030 L/s/m). At TR = 5 years, all ports except Jebha exhibit overtopping. However, only Kabila (0.007–47.23 L/s/m), Chmaala (0.001–1.48 L/s/m), and Cala Iris (0.004–3.13 L/s/m) surpass safety thresholds. For TR = 25 years, all ports experience overtopping, most notably Kabila (0.001–240.43 L/s/m), Chmaala (0.03–66.79 L/s/m), and Cala Iris (0.41–44.90 L/s/m). Among the remaining ports, Fnideq stays below threshold (max 0.01 L/s/m), while M'diq and Al Hoceima exceed 1 L/s/m, and Marina Smir and Jebha exceed 0.3 L/s/m but remain below 1 L/s/m.

Figure 4 shows overtopping projections for a 1-year TR in 2100. The top row corresponds to scenario SSP2-4.5, the bottom to SSP5-8.5; columns represent lower, mean, and upper sea level rise (SLR) estimates.

Under SSP2-4.5, the lower SLR band results in negligible discharges at all ports, with the highest being 0.13 L/s/m at Kabila (maximum Hs). With the mean SLR, only Kabila reaches the 0.3 L/s/m threshold for the maximum Hs. All other discharges remain under 0.1 L/s/m, except Cala Iris at 0.16 L/s/m. With upper SLR, significant discharges again appear only in Kabila (0.49 L/s/m) and Cala Iris (0.33 L/s/m), both for the maximum Hs.

SSP5-8.5 shows a similar trend: negligible overtopping in most ports. Cala Iris exceeds 0.3 L/s/m only with upper SLR—0.35 L/s/m (ensemble Hs) and 0.53 L/s/m (maximum Hs). Kabila shows 0.58 L/s/m for maximum Hs under lower SLR, 0.37 L/s/m (ensemble Hs) and 1.31 L/s/m (maximum Hs) under mean SLR, and 0.57 L/s/m (ensemble Hs) and 2.11 L/s/m (maximum Hs) under upper SLR.

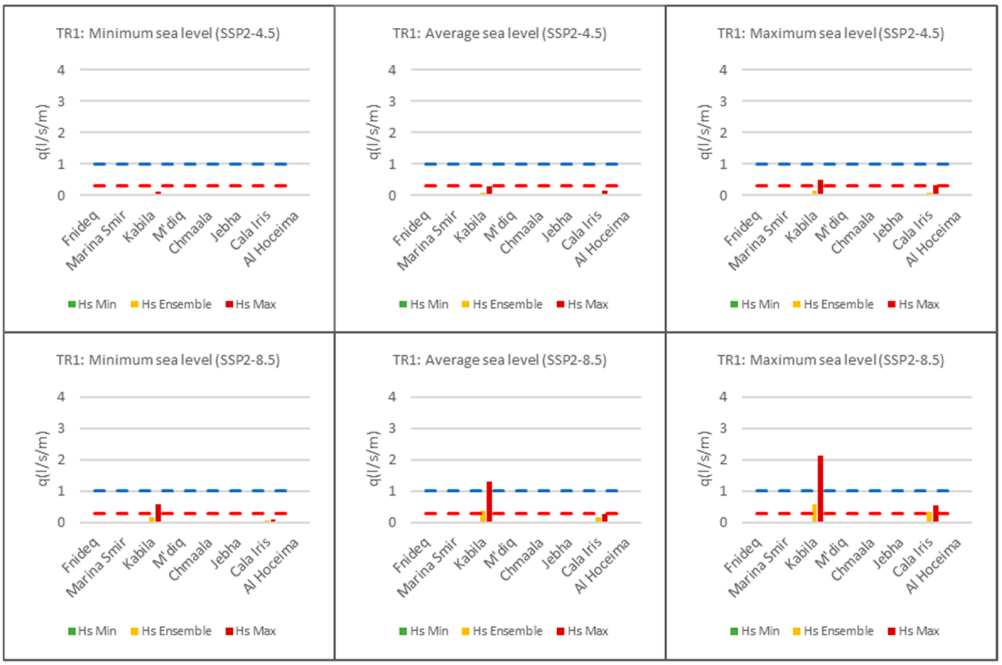

Figure 4. Overtopping discharges *q* for a return period of 1 year and the two future scenarios: SSP2-4.5 (upper row) and SSP5-8.5 (lower row). The left column represents the values for the lower confidence band of SLR, the central column represents the mean estimate, and the right column represents the upper confidence band. The colors and dashed lines have the same meaning as in Figure 3.

Figure 5 presents results for a 5-year TR. Only three ports—Kabila, Cala Iris, and Chmaala—exceed tolerable thresholds in both scenarios. Kabila shows the highest discharges, ranging from 3.69–16.27 L/s/m (ensemble *Hs*) to 9.61–48.88 L/s/m (maximum *Hs)*. Cala Iris ranges from 0.96–5.91 L/s/m (ensemble *Hs*) to 10.45 L/s/m (maximum *Hs*). Chmaala varies from 0.23–0.86 L/s/m (ensemble *Hs*) to 1.01–2.98 L/s/m (maximum *Hs*).

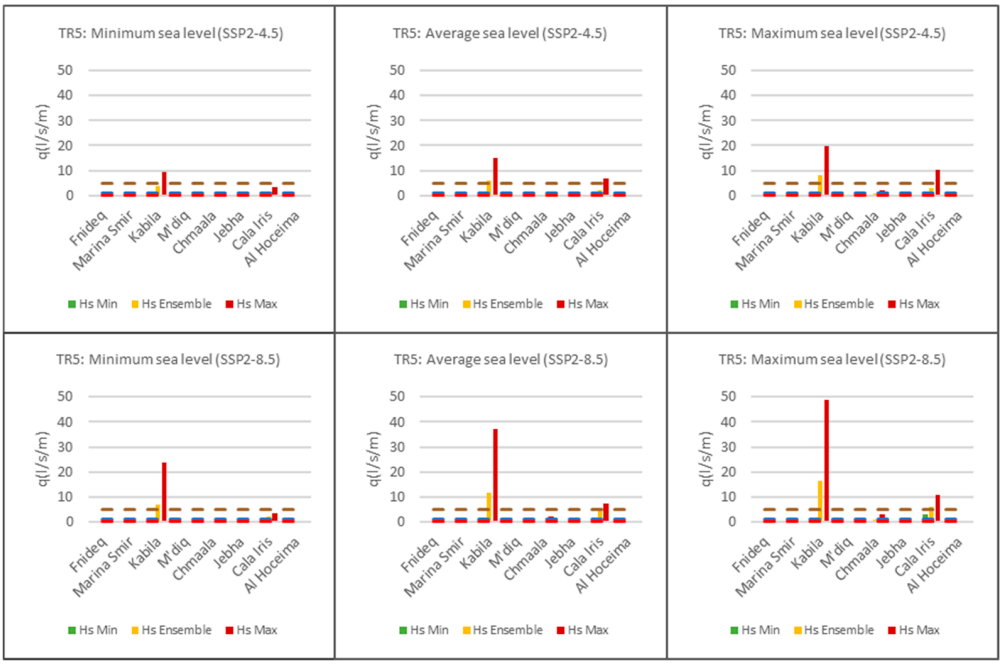

Figure 5. Overtopping discharges *q* for a return period of 5 years and the two future scenarios: SSP2-4.5 (upper row) and SSP5-8.5 (lower row). The left column illustrates the values for the lower confidence band of SLR, the central column illustrates the mean estimate, and the right column illustrates the upper confidence band. The colors and dashed lines have the same meaning as in Figure 3.

Figure 6 displays results for a 25-year TR. All ports except Fnideq exceed tolerable discharges and fall into three groups:

i. High-impact ports: Kabila, Chmaala, and Cala Iris. For the upper *Hs* band, these exceed 100 L/s/m.
   - o Kabila: Discharges range from 61.6–151.0 L/s/m (ensemble *Hs*) to 292.8–508.7 L/s/m (maximum *Hs*), though often negligible with lower *Hs*.
   - o Chmaala: 21.3–50.4 L/s/m (ensemble *Hs*) to 147.1–222.0 L/s/m (maximum *Hs*).
   - o Cala Iris: 15.9–32.2 L/s/m (ensemble *Hs*) to 92.7–165.3 L/s/m (maximum *Hs*).

ii. Moderate-impact ports: M'diq, Jebha, and Al Hoceima show overtopping above 5 L/s/m in some scenarios but lower magnitudes in others.
   - o M'diq: 1.0–1.9 L/s/m (ensemble *Hs*) to 7.8–14.6 L/s/m (maximum *Hs*).
   - o Jebha and Al Hoceima: Slightly lower but within a comparable range.

iii. Low-impact port: Marina Smir. While overtopping exceeds the 0.3 and 1.0 L/s/m thresholds under upper *Hs* bands (0.9–2.2 L/s/m), it does not reach the critical 5 L/s/m level.

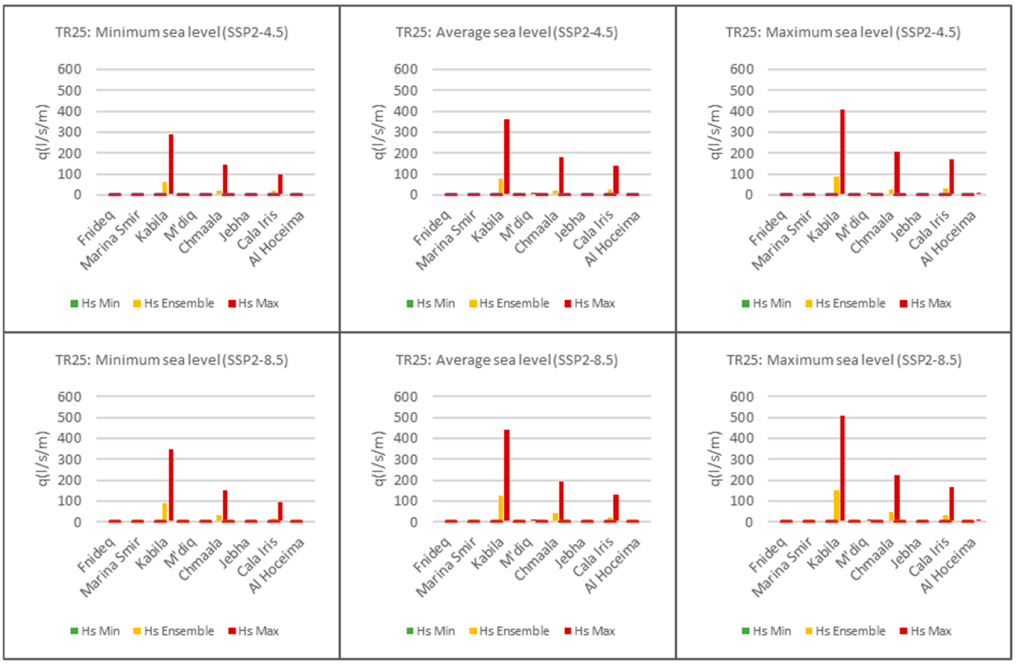

Figure 6. Overtopping discharges q for a return period of 25 years and the two future scenarios: SSP2-4.5 (upper row) and SSP5-8.5 (lower row). The left column illustrates the values for the lower confidence band of SLR, the central column illustrates the mean estimate, and the right column illustrates the upper confidence band. The colors and dashed lines have the same meaning as in Figure 3.

Table 1 presents a summary of the results for each port and scenario, ranking them by their level of vulnerability according to the following scale:

- $q \leq 0.3$ L/s/m, no vulnerability (0).
- $0.3 < q \leq 1$ L/s/m, very low vulnerability (1).
- $1 < q \leq 5$ L/s/m, low vulnerability (2).
- $5 < q \leq 20$ L/s/m, moderate vulnerability (3).
- $q > 20$ L/s/m, high vulnerability (4).

It is worth noting that, all else being equal, the differences in results between the SSP2-4.5 and SSP5-8.5 scenarios are relatively small for most ports, with values remaining within the same order of magnitude. This is primarily because the projected sea level rise

(SLR) between the two scenarios differs by only about 20 cm, and the wave projections also show no significant variation between them.

Table 1. Vulnerability levels of the ports across scenarios.

Port	TR 1 Year		TR 5 Years		TR 25 Years	
	SSP2-4.5	SSP5-8.5	SSP2-4.5	SSP5-8.5	SSP2-4.5	SSP5-8.5
Fnideq	0	0	0	0	0	0
Marina Smir	0	0	0	0	2	2
Kabila	1	1	3	4	4	4
M'diq	0	0	0	0	3	3
Chmaala	0	0	2	2	4	4
Jebha	0	0	0	0	3	3
Cala Iris	1	2	3	3	4	4
Al Hoceima	0	0	0	0	3	3

4. Discussion

A key distinction of this study is its integration of multiple wave height models and a broad range of sea level rise (SLR) projections. While most research relies on a single wave model, this study uses four, capturing inter-model variability and better representing future uncertainties. This multi-model framework provides a more robust analysis of overtopping discharge, addressing limitations of single-model studies that may not reflect the full spectrum of future conditions. Additionally, rather than focusing solely on average projections, this study incorporates minimum, maximum, and mean values for both wave height (H_s) and SLR, enabling a comprehensive assessment of future scenarios and associated uncertainties.

As expected, overtopping discharge (q) increases from the 1-year to the 5-year and 25-year return periods, indicating heightened risks for more intense events. This trend underscores the vulnerability of port infrastructure under both SSP2-4.5 and SSP5-8.5 scenarios as wave energy and sea levels rise. For the 25-year return period, q values often exceed critical thresholds, pointing to a high likelihood of frequent overtopping. Even at the 5-year return period, ports like Kabila and Chmaala already show median discharges surpassing safety limits, suggesting these locations could face overtopping under relatively moderate storms. While most ports show less overtopping at the 1-year return period, three out of eight (37.5%) still exceed minimum thresholds, indicating that risks exist even for frequent events.

The interquartile range (IQR) of q generally widens with longer return periods, reflecting increased variability and growing uncertainty in discharge predictions. This is largely due to the expanded range of combinations between SLR and H_s that lead to significant overtopping events at higher return periods.

The results also reveal significant variability in overtopping discharge across ports, driven by differences in wave conditions and SLR. Figure 7 illustrates this through box plots showing the full distribution of q values at each port and return period.

Each plot includes the minimum, maximum, median, and the 25th and 75th percentiles based on all combinations of H_s and SLR. In total, 26 different H_s values and six water level scenarios (three from each RCP pathway: mean, upper, and lower confidence bands) were combined, yielding 156 q values per return period, which were further expanded by the number of wave directions affecting each port.

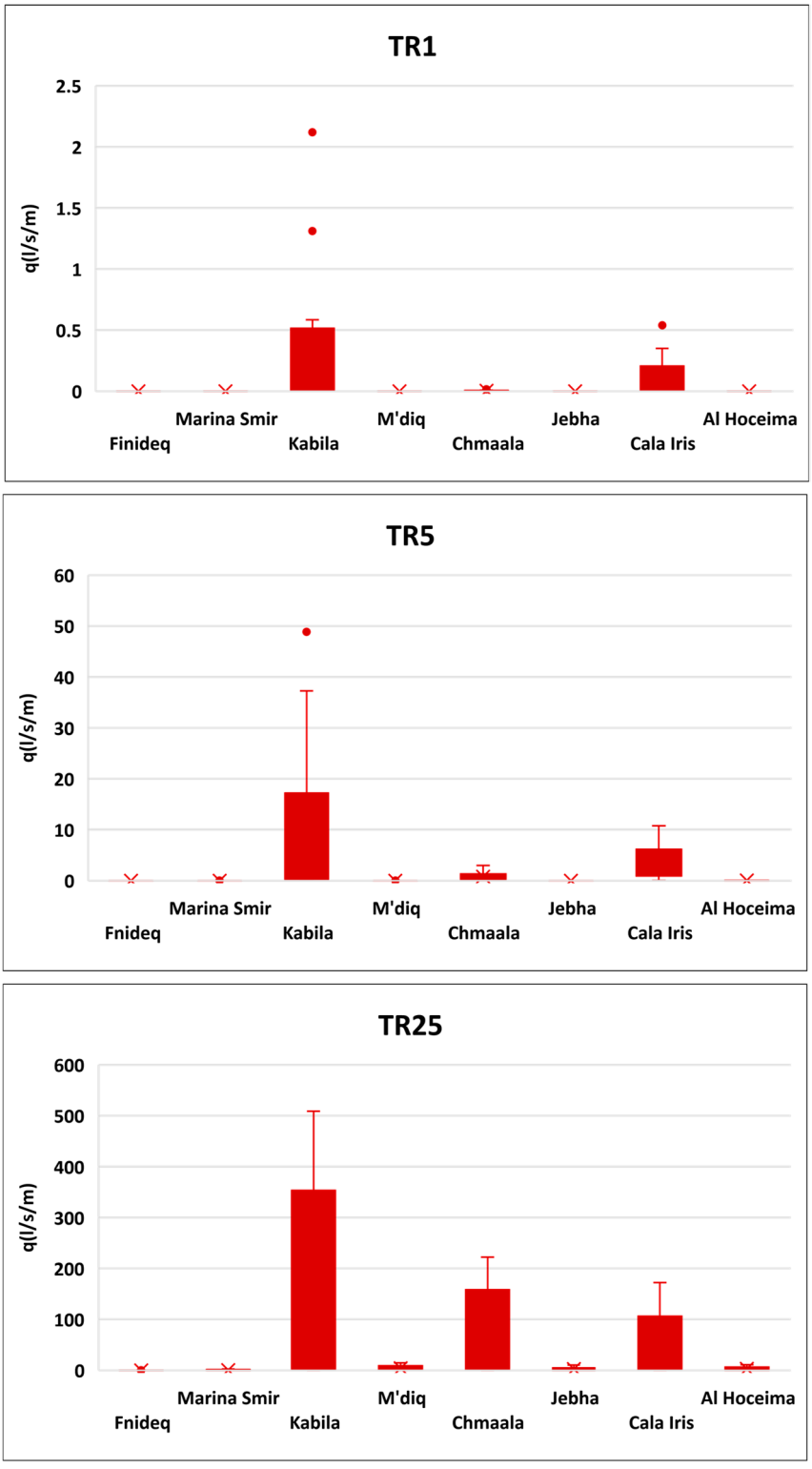

Figure 7. Box plots showing the distribution of overtopping discharges in all ports for the three return periods considered: 1 year (top panel), 5 years (middle panel), and 25 years (bottom panel). Points beyond the whiskers correspond to outliers.

It should be noted that overtopping discharges at Chmaala Port are higher than those at Cala Iris for TR25, whereas for TR1 and TR5, they are lower. This behavior arises because, when wave propagation is simulated using the SWAN model, the combined effect of local bathymetry and wave periods occasionally leads to higher significant wave heights (*Hs*) at the toe of the port breakwater.

In most ports (6 out of 8), the spread of the box plots—especially the whiskers—widens with increasing return periods, indicating higher variability in q over time. This greater spread emphasizes the difficulty in predicting overtopping events and highlights the need to assess both lower and upper extremes to capture the full range of potential infrastructure impacts.

Table 2 reinforces this point by summarizing the ratio between maximum and minimum q values when either SLR or H_s is varied while keeping the other constant.

Table 2. Ratio between the maximum and the minimum discharge considering SLR variable (with the same H_s) and H_s variable (with the same SLR). Empty cells indicate that overtopping discharges are negligible.

Port	TR1		TR5		TR25	
	SLR Variable	Hs Variable	SLR Variable	Hs Variable	SLR Variable	Hs Variable
Fnideq	-	-	-	-	-	-
M. Smir	-	-	-	-	1.6–1.8	6.6–10.4
Kabila	3.3–3.9	1.6–3.8	2.1–4.8	82–215	1.4–1.6	116–4504
M'diq	-	-	-	-	1.6–3.0	122–212
Chmaala	-	-	1.4–2.9	20−245	1.2–3.1	288–4454
Jebha	-	-	-	-	2.1–5.7	92−223
Cala Iris	6.9–7.0	24–31	2.9–5.9	3.4–115	1.7–2.0	118–177
Al Hoceima	-	-	-	-	2.0–3.4	99–171

Only discharges above 0.01 L/s/m are included to avoid distortion from negligible values. Two key trends emerge:

i. When only SLR is varied, q variability decreases with increasing return period.
ii. When only H_s is varied, q variability increases with return period.

Specifically, for variable SLR and fixed H_s, the variability in q remains within a single order of magnitude: ratios range from 3.3 to 7.0 (TR = 1), 1.4 to 5.9 (TR = 5), and 1.2 to 5.7 (TR = 25). In contrast, with variable H_s and fixed SLR, the ratios are substantially larger, often spanning two to three orders of magnitude: 1.6–31 (TR = 1), 3.4–245 (TR = 5), and 6.6–4504 (TR = 25). This indicates that H_s fluctuations have a significantly greater influence on overtopping discharge than SLR changes.

These results are consistent with those of Kerpen et al. [51], who observed that overtopping discharges could be robustly estimated for water level changes but, in contrast, changes in wave parameters led to substantial discrepancies in overtopping volumes. In addition, these findings align with the broader scientific understanding that projections of future wave climate carry high uncertainty due to climate change [52].

This is because wave parameters are influenced by a range of atmospheric processes (e.g., winds and storms), oceanic processes (e.g., currents, tropical cyclones, and residual waves), and local bathymetry. Even small errors in wind fields, wave energy dissipation, or local sea conditions can substantially affect the resulting projections. Consequently, uncertainty is largely dominated by inter-model variability in climate simulations, while single-model studies fail to capture up to approximately 50% of the total associated uncertainty [53,54]. Several authors [55] have reported that model-to-model variability often exceeds that arising from emission scenario differences.

In contrast, sea-level rise (SLR) projections are primarily governed by comparatively well-understood processes, such as glacier melt, thermal expansion, and land subsidence. Although uncertainties remain, these processes operate over longer temporal scales and exhibit less spatial variability. Wave dynamics, on the other hand, involve high spatial

and temporal variability; therefore, accurately projecting future wave conditions requires high-resolution modeling, which is not always feasible [56].

Other studies also highlight the variability of wave projections [57,58]. Although SLR estimates are more robust, they still depend heavily on the selected climate scenario and are affected by uncertainties such as the potential melting of the Greenland and Antarctic ice sheets [59]. However, the results are also counterintuitive, as there is a consensus that, in the Mediterranean region, maximum waves and storm surges will decrease, while the mean level will increase [60,61]. The models employed in this study are consistent with the broader regional trend, as they indicate an average decrease in *Hs* of between 0.9% and 2% across the study area, although slight increases in *Hs* are observed toward the west, near the Strait of Gibraltar [62]. Nevertheless, the combination of slightly lower *Hs* and higher sea levels results in greater overtopping discharges.

In summary, the combination of larger uncertainties in wave projections and their significantly greater influence on q values makes accurate estimation of future H_s more critical than precise SLR predictions for overtopping assessments. Therefore, to improve the reliability of coastal risk assessments, future research must focus on refining wave projection models. Enhanced accuracy in wave forecasts will help stakeholders better anticipate potential risks and design more effective adaptation strategies for vulnerable coastal infrastructure.

From a broader perspective, these findings highlight the importance of considering both sea level rise and wave climate variability when assessing overtopping risks at coastal infrastructure such as port breakwaters. They suggest that uncertainties in wave heights may exert an even greater influence on projected overtopping discharges than sea level rise.

This underscores the value of using multi-model wave projections and incorporating a wide range of sea level scenarios, particularly when planning for long-term port operability, management, and resilience.

Advancing this area of research will be critical for informing effective adaptation strategies and engineering guidelines, not only for Moroccan ports, but also for other vulnerable coastal infrastructures facing climate-driven challenges.

Future studies should prioritize improving the accuracy of regional wave climate projections and investigating compound events that combine sea level rise, storm surges, and changing wave patterns.

On the other hand, several limitations of the study should be acknowledged. A key issue concerns the combined use of AR5 wave data and AR6 sea-level rise (SLR) projections. While AR5 relies on Representative Concentration Pathways (RCPs), AR6 employs Shared Socioeconomic Pathways (SSPs). The AR6 projections generally provide higher spatial resolution and incorporate improved representations of certain processes (e.g., ice-sheet dynamics), which may lead to discrepancies between AR5- and AR6-based estimates. Nevertheless, some authors [63] have noted that median SLR values are broadly consistent across both assessments, with only relatively minor differences in overall uncertainty by 2100. Moreover, given the current absence of suitable regional-scale AR6 wave projections, other studies [64] have adopted a similar mixed approach, emphasizing that although this strategy introduces additional sources of uncertainty, the use of equivalent radiative forcing helps minimize inconsistencies. In addition, Marino et al. [64] report that wind patterns over the Mediterranean remain largely consistent between AR5 and AR6, suggesting that the primary drivers of wave generation are unlikely to change significantly.

Another limitation of the study concerns the use of an empirical formula to estimate the peak period (*Tp*) as a function of the significant wave height (*Hs*). While such relationships are widely applied [6,20] and generally acceptable under present conditions, their validity in future scenarios remains uncertain, as the *Tp*–*Hs* relationship may evolve and introduce

additional uncertainty in wave period assessments. Although *Tp* is not directly included in the formula used to calculate overtopping, variations in wave period influence wave propagation patterns, which in turn affect *Hs*. Nonetheless, studies based on projected wave data for this region [62] indicate only minor changes in mean wave period—ranging from −0.2% to 1.4% depending on the scenario—suggesting that the resulting effects on *Hs* are likely negligible.

It should be noted that the scenarios considered here are the most commonly employed in climate change analyses. Nevertheless, the potential collapse of ice sheets could give rise to more extreme, though physically plausible, scenarios, albeit with a very low probability of occurrence (<5% by 2100) [65]. Under such conditions, several studies project substantially higher mean sea-level rises by 2100—up to 1.86 m [57,66] or even 2 m [67]—which would result in significantly greater overtopping, in some cases exceeding an order of magnitude, as evidenced by analogous studies conducted in other regions of the Mediterranean [20].

Finally, it is worth highlighting that three ports—Kabila, Chmaala, and Cala Iris—are expected to be the most affected by overtopping, with discharge values exceeding critical thresholds under all storm conditions (except Chmaala for TR = 1 year). These ports, therefore, require the most urgent attention and the prompt design of adaptation measures. In contrast, the remaining ports are only expected to exceed threshold discharge levels during exceptional storm events. With these considerations, the authorities of the three most affected ports can begin planning targeted adaptation measures, including the following:

- Construction of a vertical wall at the crest of the breakwater, potentially incorporating a bullnose.
- Increase in the freeboard of the breakwater by raising its crest elevation.
- Smoothing of the breakwater slope.
- Construction of a berm in the breakwater.
- Installation of a submerged dike in front of the breakwater.

All these engineering interventions are intended to reduce overtopping discharge and must be designed with appropriate specifications to ensure the required level of reduction. Furthermore, early warning systems—such as the one described in [68]—could also be implemented to detect emerging critical situations and enable the timely adoption of preventive measures.

5. Conclusions

This study presents an investigation into the effects of climate change on wave overtopping discharge (q) across eight ports located on the Mediterranean coast of Morocco, considering two climate scenarios, SSP2-4.5 and SSP5-8.5, and horizon 2100. To represent the spectrum of possible future conditions and address inter-model variability, wave data obtained from four different models were used. The analysis was conducted for three distinct return periods, 1, 5, and 25 years, and is focused on the uncertainty associated with predict overtopping discharges from wave and SLR projections. For this reason, in addition to the central values, the data associated with the 90% confidence bands were taken into account.

Results show that overtopping discharges increase with the return period, as could be expected, and, as a consequence, the number of ports affected by excessive overtopping also increases. Thus, for TR = 1 year, two ports show discharges that exceed the tolerable thresholds. For TR = 5 years, there are three ports with potential problems due to excessive overtopping. For TR = 25 years, all but one of the ports could be affected.

Assuming the same H_s and varying SLR (considering different climate scenarios, or values corresponding to the central estimate or 90% confidence levels), the overtopping discharges show a range of variation smaller than one order of magnitude, with ratios

between the maximum and the minimum discharges between 1.2 and 7. If the same SLR is considered, varying H_s (due to the scenarios or the confidence level), the aforementioned ratio reaches values indicating changes of two or three orders of magnitude. Therefore, the selection of accurate H_s values is more critical than that of SLR to determine overtopping discharges. This illustrates the need for increased efforts to achieve better and less uncertain future wave projections.

Lastly, it should be noted that port authorities must develop adaptation plans, particularly for the three ports most affected by significant overtopping discharges—Kabila, Chmaala, and Cala Iris. The projected values not only pose operational risks but also indicate a potential for serious structural damage to the breakwaters at these ports.

Author Contributions: Conceptualization, J.P.S. and C.M.; methodology, J.P.S., X.G. and C.M.; software, R.J., X.G., D.G.-M. and P.L.; validation, R.J., X.G., D.G.-M. and P.L.; formal analysis, J.P.S., X.G. and C.M.; investigation, R.J., J.P.S. and X.G.; resources, C.M. and D.G.-M.; data curation, R.J. and P.L.; writing—original draft preparation, R.J. and J.P.S.; writing—review and editing, R.J., J.P.S., X.G. and C.M.; visualization, R.J., J.P.S. and X.G.; supervision, J.P.S. and C.M.; project administration, C.M. and D.G.-M.; funding acquisition, D.G.-M. All authors have read and agreed to the published version of the manuscript.

Funding: This research received no external funding.

Data Availability Statement: Publicly available datasets used in this study include sea level rise projections from NASA's IPCC AR6 Sea Level Projection Tool (https://sealevel.nasa.gov/ipcc-ar6-sea-level-projection-tool, accessed on 15 January 2025), tide gauge records from Puertos del Estado (https://www.puertos.es, accessed on 4 February 2025), regional wave model outputs from Med-CORDEX (provided by the institutes units in the section wave and SLR data), and bathymetric data from GEBCO (https://www.gebco.net/, accessed on 18 December 2024). Offshore wave period estimates were derived using Puertos del Estado's empirical formula, with buoy data from Melilla (https://bancodatos.puertos.es/BD/informes/extremales/EXT_1_1_1560.pdf, accessed on 4 February 2025). Access to some regional wave datasets may require institutional collaboration or direct request to the data providers. Detailed breakwater geometry data were obtained under confidentiality agreements with Moroccan governmental authorities and are not publicly available. Data corresponding to calculations carried out during this study are available from the corresponding author upon request.

Acknowledgments: The authors wish to acknowledge Puertos del Estado for providing some data used in the study. The support of the Departament de Recerca i Universitats de la Generalitat de Catalunya (Ref. 2021SGR00600) is also acknowledged.

Conflicts of Interest: The authors declare no conflicts of interest. The funders had no role in the design of the study; in the collection, analyses, or interpretation of data; in the writing of the manuscript; or in the decision to publish the results.

Abbreviations

The following abbreviations are used in this manuscript:

AR6	Sixth Assessment Report
CNRM	Centre National de Recherches Météorologiques
CMCC	Centro Euro-Mediterraneo sui Cambiamenti Climatici
CMIP6	Coupled Model Intercomparison Project Phase 6
GEBCO	General Bathymetric Chart of the Oceans
GUF	Goethe University Frankfurt
Hs	Significant Wave Height
IPCC	Intergovernmental Panel on Climate Change
LMD	Laboratoire de Météorologie Dynamique

Med-CORDEX	Mediterranean Coordinated Regional Downscaling Experiment
NASA	National Aeronautics and Space Administration
RCP	Representative Concentration Pathway
SLR	Sea Level Rise
Tp	Peak Wave Period
TR	Return Period

References

1. Verschuur, J.; Koks, E.E.; Hall, J.W. Port disruptions due to natural disasters: Insights into port and logistics resilience. *Transp. Res. D Transp. Environ.* **2020**, *85*, 102393. [CrossRef]
2. Becker, A.; Inoue, S.; Fischer, M.; Schwegler, B. Climate change impacts on international seaports: Knowledge, perceptions, and planning efforts among port administrators. *Clim. Change* **2012**, *110*, 5–29. [CrossRef]
3. Izaguirre, C.; Losada, I.J.; Camus, P.; González-Lamuño, P.; Stenek, V. Seaport climate change impact assessment using a multi-level methodology. *Marit. Policy Manag.* **2020**, *47*, 544–557. [CrossRef]
4. Van Houtven, G.; Gallaher, M.; Woollacott, J.; Decker, E. *Act Now or Pay Later: The Costs of Climate Inaction for Ports and Shipping*; Environmental Defense Fund and RTI International: Research Triangle Park, NC, USA, 2022.
5. Loh, H.S.; Zhou, Q.; Thai, V.V.; Wong, Y.D.; Yuen, K.F. Fuzzy comprehensive evaluation of port-centric supply chain disruption threats. *Ocean Coast. Manag.* **2017**, *148*, 53–62. [CrossRef]
6. Sierra, J.P.; Genius, A.; Lionello, P.; Mestres, M.; Mösso, C.; Marzo, L. Modelling the impact of climate change on harbour operability: The Barcelona port case study. *Ocean Eng.* **2017**, *141*, 64–78. [CrossRef]
7. Yang, Y.; Ge, Y. Adaptation strategies for port infrastructure and facilities under climate change at the Kaohsiung port. *Transp. Policy* **2020**, *97*, 232–244. [CrossRef]
8. Cramer, W.; Guiot, J.; Fader, M.; Garrabou, J.; Gattuso, J.; Iglesias, A.; Lange, A.; Lionello, P.; Llasat, M.; Paz, S.; et al. Climate change and interconnected risks to sustainable development in the Mediterranean. *Nat. Clim. Change* **2018**, *8*, 972–980. [CrossRef]
9. Izaguirre, C.; Losada, I.J.; Camus, P.; Vigh, J.L.; Stenek, V. Climate change risk to global port operations. *Nat. Clim. Change* **2021**, *11*, 14–20. [CrossRef]
10. Snoussi, M.; Ouchani, T.; Niazi, S. Vulnerability assessment of the impact of sea-level rise and flooding on the Moroccan coast: The case of the Mediterranean eastern zone. *Estuar. Coast. Shelf Sci.* **2008**, *77*, 206–213. [CrossRef]
11. Khouakhi, A.; Snoussi, M.; Niazi, S.; Raji, O. Vulnerability assessment of Al Hoceima bay (Moroccan Mediterranean coast): A coastal management tool to reduce potential impacts of sea-level rise and storm surges. *J. Coast. Res.* **2013**, *SI65*, 968–973. [CrossRef]
12. Agharroud, K.; Puddu, M.; Ivčević, A.; Satta, A.; Kolker, A.S.; Snoussi, M. Climate risk assessment of the Tangier-Tetouan-Al Hoceima coastal Region (Morocco). *Front. Mar. Sci.* **2023**, *10*, 1176350. [CrossRef]
13. Zittis, G.; Almazroui, M.; Alpert, P.; Ciais, P.; Cramer, P.; Dahdal, Y.; Fnais, M.; Francis, D.; Hadjinicolaou, P.; Jrrar, A.; et al. Climate change and weather extremes in the Eastern Mediterranean and Middle East. *Rev. Geophys.* **2022**, *60*, e2021RG000763. [CrossRef]
14. Gracia, V.; Sierra, J.P.; Gómez, M.; Pedrol, M.; Sampé, S.; García-León, M.; Gironella, X. Assessing the impact of sea level rise on port operability using LiDAR-derived digital elevation models. *Remote Sens. Environ.* **2019**, *232*, 111318. [CrossRef]
15. Jebbad, R.; Sierra, J.P.; Mösso, C.; Mestres, M.; Sanchez-Arcilla, A. Assessment of harbour inoperability and adaptation cost due to sea level rise. Application to the port of Tangier-Med (Morocco). *Appl. Geogr.* **2022**, *138*, 102623. [CrossRef]
16. Sierra, J.P.; Sánchez-Arcilla, A.; Gironella, X.; Gracia, V.; Altomare, C. Impact of climate change on berthing areas in ports of the Balearic Islands: Adaptation measures. *Front. Mar. Sci.* **2023**, *10*, 1124763. [CrossRef]
17. Sánchez-Arcilla, A.; Sierra, J.P.; Brown, S.; Casas-Prat, M.; Nicholls, R.J.; Lionello, P.; Conte, D. A review of potential physical impacts on harbours in the Mediterranean Sea under climate change. *Reg. Environ. Change* **2016**, *16*, 2471–2484. [CrossRef]
18. Weisse, R.; Storch, H. *Marine Climate and Climate Change: Storms, Wind Waves and Storm Surges*; Springer: Chichester, UK, 2009. [CrossRef]
19. Sierra, J.P.; Casas-Prat, M. Analysis of potential impacts on coastal areas due to changes in wave conditions. *Clim. Change* **2014**, *124*, 861–876. [CrossRef]
20. Sierra, J.P.; Casanovas, I.; Mösso, C.; Mestres, M.; Sánchez-Arcilla, A. Vulnerability of Catalan (NW Mediterranean) ports to wave overtopping due to different scenarios of sea level rise. *Reg. Environ. Change* **2016**, *16*, 1457–1468. [CrossRef]
21. Pillai, K.; Lemckert, C.; Etemad-Shadidi, A.; Cappietti, L.; Sigurdarson, S. Effect of the sea level rise on the wave overtopping rate at berm breakwater. *J. Waterw. Port Coast. Ocean Eng.* **2019**, *145*, 04019019. [CrossRef]
22. Pepi, Y.; Streicher, M.; Ricci, C.; Franco, L.; Bellotti, G. The effect of variations in water level on wave overtopping discharge over a dike: An experimental model study. *Coast. Eng.* **2022**, *178*, 104199. [CrossRef]

23. Altomare, C.; Gironella, X.; Suzuki, T.; Viccione, G.; Saponieri, A. Overtopping metrics and coastal safety: A case of study from the Catalan Coast. *J. Mar. Sci. Eng.* **2020**, *8*, 556. [CrossRef]
24. Koosheh, A.; Etemad-Shahidi, A.; Cartwright, N.; Tomlinson, R.; Van Gent, M.R. Wave overtopping layer thickness on the crest of rubble mound seawalls. *Coast. Eng.* **2023**, *188*, 104441. [CrossRef]
25. Pillai, K.; Etemad-Shadidi, A.; Lemckert, C. Wave overtopping at berm breakwaters: Review and sensitivity analysis of prediction models. *Coast. Eng.* **2017**, *120*, 1–21. [CrossRef]
26. Van der Meer, J.M.; Van Gent, M.R.A. Wave overtopping over coastal structures with oblique wind and swell waves. *J. Mar. Sci. Eng.* **2018**, *6*, 149. [CrossRef]
27. Chen, W.; Marconi, A.; Van Gent, M.R.A.; Warmink, J.J.; Hulscher, S.J.M.H. Experimental study on the influence of berms and roughness on wave overtopping at rock-armoured dikes. *J. Mar. Sci. Eng.* **2020**, *8*, 446. [CrossRef]
28. Van der Meer, J.W.; Allsop, N.W.; Bruce, T.; De Rouck, J.; Kortenhaus, A.; Pullen, T.; Schüttrumpf, H.; Troch, P.; Zanuttigh, B. *Manual on Wave Overtopping of Sea Defences and Related Structures*; TU Delft: Delft, The Netherlands, 2016. Available online: www.overtopping-manual.com (accessed on 24 July 2025).
29. Romano, A.; Bellotti, G.; Briganti, R.; Franco, L. Uncertainties in the physical modelling of the wave overtopping over a rubble mound breakwater: The role of the seeding number and of the test duration. *Coast. Eng.* **2015**, *103*, 15–21. [CrossRef]
30. Molines, J.; Herrera, M.P.; Gómez-Martín, M.E.; Medina, J.R. Distribution of individual wave overtopping volumes on mound breakwaters. *Coast. Eng.* **2019**, *149*, 15–27. [CrossRef]
31. Mares-Nasarre, P.; Van Gent, M.R.; Morales-Nápoles, O. A copula-based model to describe the uncertainty of overtopping variables on mound breakwaters. *Coast. Eng.* **2024**, *189*, 104483. [CrossRef]
32. Gao, J.; Ma, X.; Zang, J.; Dong, G.; Zhu, Y.; Zhou, L. Numerical investigation of harbor oscillations induced by focused transient wave groups. *Coast. Eng.* **2020**, *158*, 103670. [CrossRef]
33. Gao, J.; Ma, X.; Dong, G.; Chen, H.; Liu, Q.; Zang, J. Investigation on the effects of Bragg reflection on harbor oscillations. *Coast. Eng.* **2021**, *170*, 103977. [CrossRef]
34. Gao, J.; Hou, L.; Liu, Y.; Shi, H. Influences of Bragg reflection on harbor resonance triggered by irregular wave groups. *Coast. Eng.* **2024**, *305*, 117941. [CrossRef]
35. Sierra, J.P. Economic impact of overtopping and adaptation measures in Catalan ports due to sea level rise. *Water* **2019**, *11*, 1440. [CrossRef]
36. Chini, N.; Stansby, P.K. Extreme values of coastal wave overtopping accounting for climate change and sea level rise. *Coast. Eng.* **2012**, *65*, 27–37. [CrossRef]
37. Hilmi, K.; Koutitonsky, V.G.; Orbi, A.; Lakhdar, J.I.; Chagdali, M. Oualidia lagoon, Morocco: An estuary without a river. *Afr. J. Aquat. Sci.* **2005**, *30*, 1–10. [CrossRef]
38. Gouvernement du Maroc. *Bulletin Officiel du Maroc*; Gouvernement du Maroc: Rabat, Morocco, 2016.
39. Raji, O.; Dezileau, L.; Von Grafenstein, U.; Niazi, S.; Snoussi, M.; Martinez, P. Extreme sea events during the last millennium in the northeast of Morocco. *Nat. Hazards Earth Syst. Sci.* **2015**, *15*, 203–211. [CrossRef]
40. El Mrini, A.; Anthony, E.J.; Maanan, M.; Taaouati, M.; Nachite, D. Beach-dune degradation in a Mediterranean context of strong development pressures, and the missing integrated management. *Ocean Coast. Manag.* **2012**, *69*, 299–306. [CrossRef]
41. Lionello, P.; Boldrin, U.; Giorgi, F. Future changes in cyclone climatology over Europe as inferred from a regional climate simulation. *Clim. Dyn.* **2008**, *30*, 657–671. [CrossRef]
42. Lira-Loarca, A.; Ferrari, F.; Mazzino, A.; Besio, G. Future wind and wave energy resources and exploitability in the Mediterranean Sea by 2100. *Appl. Energy* **2021**, *302*, 117492. [CrossRef]
43. Reale, M.; Cabos Narvaez, W.; Cavicchia, L.; Conte, D.; Coppola, E.; Flaounas, E.; Giorgi, F.; Gualdi, S.; Hochman, A.; Li, L.; et al. Future projections of Mediterranean cyclone characteristics using the Med-CORDEX ensemble of coupled regional climate system models. *Clim. Dyn.* **2022**, *58*, 2501–2524. [CrossRef]
44. Casas-Prat, M.; Sierra, J.P. Projected future wave climate in the NW Mediterranean Sea. *J. Geophys. Res. Oceans* **2013**, *118*, 3548–3568. [CrossRef]
45. Intergovernmental Panel on Climate Change (IPCC). Contribution of Working Group I to the Sixth Assessment Report of the Intergovernmental Panel on Climate Change. In *Climate Change 2021: The Physical Science Basis*; Cambridge University Press: Cambridge, UK; New York, NY, USA, 2021. [CrossRef]
46. Ruti, P.M.; Somot, S.; Giorgi, F.; Dubois, C.; Flaounas, E.; Obermann, A.; Dell'Aquila, A.; Pisacane, G.; Harzallah, A.; Lombardi, E.; et al. Med-Cordex initiative for Mediterranean climate studies. *Bull. Am. Meteorol. Soc.* **2016**, *97*, 1187–1208. [CrossRef]
47. IPCC. *Climate Change 2013: The Physical Science Basis*; Cambridge University Press: Cambridge, UK; New York, NY, USA, 2013. [CrossRef]
48. Booij, N.; Ris, R.C.; Holthuijsen, L.H. A third-generation wave model for coastal regions: 1. Model description and validation. *J. Geophys. Res. Oceans* **1999**, *104*, 7649–7666. [CrossRef]

49. Novaczek, E.; Devillers, R.; Edinger, E.N. Generating higher resolution regional seafloor maps from crowd-sourced bathymetry. *PLoS ONE* **2019**, *14*, e0216792. [CrossRef] [PubMed]
50. Suzuki, T.; Altomare, C.; Yasuda, T.; Verwaest, T. Characterization of overtopping waves on sea dikes with gentle and shallow foreshores. *J. Mar. Sci. Eng.* **2020**, *8*, 752. [CrossRef]
51. Kerpen, N.B.; Daemrich, K.-F.; Lojek, O.; Schlurmann, T. Effect of variations in water level and steepness on the robustness of wave overtopping estimation. *J. Mar. Sci. Eng.* **2020**, *8*, 63. [CrossRef]
52. Ewans, K.; Jonathan, P. Uncertainties in estimating the effect of climate change on 100-year return value for significant wave height. *Ocean Eng.* **2023**, *272*, 113840. [CrossRef]
53. Morim, J.; Hemer, M.; Wang, X.; Cartwright, N.; Trenham, C.; Semedo, A.; Young, I.; Bricheno, L.; Camus, P.; Casas-Prat, M. Robustness and uncertainties in global multivariate wind-wave climate projections. *Nat. Clim. Change* **2019**, *9*, 711–718. [CrossRef]
54. Toomey, T.; Lira-Loarca, A.; Marcos, M.; Besio, G.; Orfila, A. Future wave climate in the Mediterranean Sea and associated uncertainty from an ensemble of 31 GCM-RCM wave simulations. *Earth's Future* **2025**, *13*, e2024EF004992. [CrossRef]
55. Wang, X.L.; Feng, Y.; Swail, V.R. Climate change signal and uncertainty in CMIP5-based projections of global ocean surface wave heights. *J. Geophys. Res.* **2015**, *120*, 3859–3871. [CrossRef]
56. Lobeto, H.; Semedo, A.; Menendez, M.; Lemos, G.; Kumar, R.; Akpinar, A.; Dobrynin, M.; Kamranzad, B. On the assessment of the wave modeling uncertainty in wave climate projections. *Environ. Res. Lett.* **2023**, *18*, 124006. [CrossRef]
57. Mori, N.; Shimura, T.; Yasuda, T.; Mase, H. Multi-model climate projections of ocean surface variables under different climate scenarios—Future change of waves, sea level and wind. *Ocean Eng.* **2013**, *71*, 122–129. [CrossRef]
58. Bitner-Gregersen, E.M.; Vanem, E.; Gramstad, O.; Horte, T.; Aarnes, O.J.; Reistad, M.; Breivik, Ø.; Magnusson, A.K.; Natvig, B. Climate change and safe design of ship structures. *Ocean Eng.* **2018**, *149*, 226–237. [CrossRef]
59. Jackson, L.P.; Jevrejeva, S. A probabilistic approach to 21st century regional sea-level projections using RCP and high-end scenarios. *Glob. Planet. Change* **2016**, *146*, 179–189. [CrossRef]
60. Lionello, P.; Cogo, S.; Galati, M.B.; Sanna, A. The Mediterranean surface wave climate inferred from future scenario simulations. *Glob. Planet. Change* **2008**, *63*, 152–162. [CrossRef]
61. Lionello, P.; Conte, D.; Marzo, L.; Scarascia, L. The contrasting effect of increasing mean sea level and decreasing storminess on the maximum water level during storms along the coast of the Mediterranean Sea in the mid 21st century. *Glob. Planet. Change* **2017**, *151*, 80–91. [CrossRef]
62. Sierra, J.P.; Castrillo, R.; Mestres, M.; Mösso, M.; Lionello, P.; Marzo, L. Impact of climate change on wave energy resource in the Mediterranean coast of Morocco. *Energies* **2020**, *13*, 2993. [CrossRef]
63. Slangen, A.B.A.; Palmer, M.D.; Camargo, C.M.L.; Church, J.A.; Edwards, T.L.; Hermans, T.H.J.; Hewitt, H.T.; Garner, G.G.; Gregory, J.M.; Kopp, R.E.; et al. The evolution of 21st century sea-level projections from IPCC AR5 to AR6 and beyond. *Camb. Prism. Coast. Futures* **2023**, *1*, e7. [CrossRef]
64. Marino, M.; Nasca, S.; Alkharoubi, A.I.; Cavallaro, L.; Foti, E.; Musumeci, R.E. Efficacy of nature-based solutions for coastal protection under a changing climate: A modelling approach. *Coast. Eng.* **2025**, *198*, 104700. [CrossRef]
65. Jevrejeva, S.; Grinsted, A.; Moore, J.C. Upper limit for sea level projections by 2100. *Environ. Res. Lett.* **2014**, *9*, 104008. [CrossRef]
66. Jevrejeva, S.; Moore, J.C.; Grinsted, A. Sea level projections to AD2500 with a new generation of climate change scenarios. *Glob. Planet. Change* **2012**, *80–81*, 14–20. [CrossRef]
67. Rahmstorf, S. A semi-empirical approach to projecting future sea-level rise. *Science* **2007**, *315*, 368–370. [CrossRef] [PubMed]
68. Sabino, A.; Rodrigues, A.; Araújo, J.; Poseiro, P.; Reis, M.T.; Fortes, C.J. Wave overtopping analysis and early warning forecast system. In *Computational Science and Its Applications—ICCSA 2014*; Murgante, B., Misra, S., Rocha, A.M.A.C., Torre, C., Rocha, J.G., Falcão, M.I., Taniar, D., Apduhan, B.O., Gervasi, O., Eds.; Lecture Notes in Computer Science; Springer: Cham, Switzerland, 2014; Volume 8579, pp. 241–255. [CrossRef]

Disclaimer/Publisher's Note: The statements, opinions and data contained in all publications are solely those of the individual author(s) and contributor(s) and not of MDPI and/or the editor(s). MDPI and/or the editor(s) disclaim responsibility for any injury to people or property resulting from any ideas, methods, instructions or products referred to in the content.